Evaporation-rate and substrate-temperature dependence of direct exciton transitions in BiI_3 thin films formed by hot-wall technique on Al_2O_3 substrates

S. Arishima[1], K. Murata[2], R. Sakamoto[1], T. Ueda[1], F. Ichikawa[3], K. Iwamitsu[2], I. Akai[*,4]

[1] Graduate school of Science and Technology, Kumamoto University, 2-39-1 Kurokami, Chuo-ku, Kumamoto 860-8555, Japan
[2] Faculty of Science, Kumamoto University, 2-39-1 Kurokami, Chuo-ku, Kumamoto 860-8555, Japan
[3] Faculty of Advanced Science and Technology, Kumamoto University, 2-39-1 Kurokami, Chuo-ku, Kumamoto 860-8555, Japan
[4] Institute of Pulsed Power Science, Kumamoto University, 2-39-1 Kurokami, Chuo-ku, Kumamoto 860-8555, Japan

Key words: BiI_3, exciton, hot-wall technique, inner exciton, interface exciton

* Corresponding author: iakai@kumamoto-u.ac.jp

Using a hot-wall technique, BiI_3 thin films were deposited on α-Al_2O_3 substrates at different evaporation rates and substrate temperatures in order to optimize these conditions. From X-ray diffraction data, it was confirmed that BiI_3 layers were regularly stacked. Absorption due to direct excitons in BiI_3 was observed in the deposited thin films. To study the translational symmetry and homogeneity of the films, changes in direct exciton transitions were examined. Direct excitons could be split into inner X^{Inner} and interface X^{Inter} excitons due to a collapse of translational symmetry along the stacking direction for a finite thickness, and the mean value $\hat{E}$ and the energy difference ΔE for the transition energies for these excitons were obtained. To evaluate the sample quality, the dependence of $\hat{E}$ and ΔE on the deposition conditions was investigated based on a tight-binding model for flake-like crystals consisting of a finite number n of BiI_3 layers. In this model, a site shift energy δ was introduced for the interfaced BiI_3 layers, which represents the difference of the on-site energy for the excitons. From the magnitude of ΔE, the BiI_3 thin films are considered to consist of packed flake-like crystals, whose translational symmetry will be maintained within four or five ($n = 4$ or 5) BiI_3 layers. From the variations of δ, it was found that an evaporation rate of about 0.8 Å/s and a substrate temperature of $75^{\circ}\mathrm{C}$ are the best conditions for BiI_3 thin film deposition on α-Al_2O_3 substrates.

1 Introduction In certain semiconductors, dipole-allowed excitonic transitions provide strong and sharp absorption lines below the fundamental absorption edges for band-to-band optical transitions [1,2]. These exciton transitions play an important role in optical nonlinear functionalities [3]. Especially, two-dimensional (2D) excitons are of great interest [4] because they have significant joint densities of states at the transition energy.

In the compound semiconductor GaAs, quantum well (QW) and superlattice [5] structures have been produced by molecular beam epitaxy (MBE) [6] and metal organic vapor phase epitaxy (MOVPE) [7]. Optical and electronic devices based on these quantum structures have become indispensable in advanced information technology. In studies of their optical responses, an optical Stark effect [8] in 2D-excitons has been reported in a GaAs-QW and it is strongly expected that this can be applied to high speed optical switching devices. In such covalent bonding semiconductors, a large dielectric constant shields the electron-hole binding in excitons and the Bohr radius becomes large. Recently, 2D-materials represented by graphene have attracted considerable attention in both condensed matter physics research and its applications [9,10]. In 2D-exciton systems in mono-layer semiconductors, various

excitonic properties are being uncovered in 2D transition metal dichalcogenides such as $MoSe_2$ [11, 12] and WSe_2 [13]. In such excitonic systems, Coulomb screening of the electron-hole binding in excitons is remarkably reduced in contrast to three-dimensional semiconductors [12, 13]. It is expected that 2D-exciton states realized at room temperature will be widely adopted in next-generation photonic and optoelectronic applications.

Stacking fault excitons (SFEs) in the layered semiconductor BiI_3 [14] are 2D-excitons having a large Coulomb binding energy between electrons and holes. In each fundamental BiI_3 layer, a bismuth layer with a honeycomb structure is sandwiched between iodine layers with a hexagonal close-packed (hcp) structure, and the BiI_3 layers are stacked along the z-axis by van der Waals bonding. During the stacking process in such layered semiconductors, stacking faults can take place [15]. In BiI_3 crystals, stacking-skidding occurs at the van der Waals interface and breaks the translational symmetry of the regular stacking and, as a result, very sharp absorption lines appear below the transition energy for indirect excitons [14, 16]. These peaks are due to 2D-excitons, which are trapped two-dimensionally at a stacking fault interface. In good quality samples crystallized by sublimation of purified BiI_3 under conditions of excess iodine gas, the in-plane uniformity of the stacking fault interface is very high and extends over square millimeters. In such samples, the absorption lines associated with the SFEs have very small spectral widths in about 0.1 meV and the lowest lying T exciton in the SFEs has a high luminescent quantum efficiency of almost unity [17]. Thus, SFEs in BiI_3 crystals are considered to be ideal 2D-excitons and various optical nonlinearities have been reported, such as optical Stark effects [18] and anomalous propagation of the quantum coherent excitonic states at the stacking fault interface [19], which has a threshold excitation density and is considered to be due to many-body effects among high density 2D-excitons. Recently, studies of the photovoltaic (PV) effect in BiI_3 thin films have been conducted. Brandt *et al.* demonstrated that the absorption edge appears at ~ 1.8 eV in their BiI_3 thin films, and such thin films are promising candidates for PV absorbers [20]. Furthermore, studies both on the optimization of BiI_3 crystal growth [21] and of electrode selection for PV application [22] have been conducted.

For applications of the layered semiconductor BiI_3, it is necessary to control thin-film crystallization by a sophisticated method comparable to MBE and MOVPE. For BiI_3 thin-film crystals, a van der Waals epitaxy growth method [23] is effective because there are no dangling bonds at the upper and lower interfaces of the BiI_3 layers, which are held together only by weak van der Waals bonds. Takeyama *et al.* [24, 25] have employed a hot-wall method, which is a van der Waals epitaxy method, using cleaved single crystals of PbI_2 and CdI_2 as substrates for stacking BiI_3 thin films. From the viewpoint of epitaxial crystal growth, these heavy-metal iodide materials are suitable as substrates. They have the same hcp structure and the atomic spacing between iodine sites in PbI_2 (4.59 Å [26]) and CdI_2 (4.24 Å [26]) are close to that in BiI_3 (4.33 Å), which is a sufficient small lattice mismatches. However, the use of such heavy-metal compounds should be avoided due to the potential hazards to human beings, other life forms and the environment.

We employed α-Al_2O_3 substrates with a (0001) surface because they are optically transparent and have a van der Waals interface. The (0001) surface has an hcp structure of aluminum atoms with an atomic spacing of 4.75 Å and a lattice mismatch with BiI_3 of less than 10%. In this research, we deposited BiI_3 on α-Al_2O_3 substrates using the hot-wall method with changing evaporation rate and substrate temperature. In addition, to optimize these conditions, variations of sample quality were studied from measurements of X-ray diffraction (XRD) and absorption spectra.

In high-quality single crystals of BiI_3, direct excitons give a strong absorption peak with an intensity exceeding 6×10^5 cm^{-1} in absorption coefficient [14]. The direct excitons also have a small Bohr radius (about 6.1 Å) comparable to the thickness of the I-Bi-I unit molecular layer (6.9 Å), reflecting the large binding energy (about 180 meV) of the exciton [14]. As a result, it is expected that direct exciton transitions are strongly influenced by homogeneity and/or inhomogeneity in the stacking and in-plane translational symmetries in BiI_3 crystals, and it has been reported that the direct exciton states split into two states in BiI_3/CdI_2 multilayer structures [27]. In this paper, we performed spectral analyses of direct exciton transitions in order to evaluate the homogeneity and/or inhomogeneity of the deposited thin-films based on a tight-binding model proposed in a previous study [27].

2 Experimental Figure 1 shows a schematic diagram of the hot-wall furnace used in the present study. Sample molecules are heated by a temperature-controlled source heater and are evaporated in a quartz crucible. The upper part of the quartz crucible is also heated with another temperature-controlled wall-heater. The sample substrate is loaded to cover the small outlet port of the crucible. The substrate block can be also heated with a temperature-controlled head-heater. The hot-wall furnace is quasi-enclosed by the heated wall and substrate. When the substrate temperature is high, unstable molecules are expected to be released from the substrate and only stable molecules remain. As a result, slow deposition is realized under quasi-thermal equilibrium.

As seed-BiI_3 crystals for evaporation, we prepared powder-like crushed single crystals. The crystals before crushing were grown by sublimation of BiI_3 under a condition of excess iodine gas. The BiI_3 was purified beforehand through several repeated sublimation processes in vacuum [28]. The seed crystals were filled in a Mexican hat-like groove in the middle of the quartz crucible

Table 1 Conditions for BiI_3 thin-film deposition: †Evaporation rate = (evaporation rate before deposition + evaporation rate after deposition) / 2, ††Deposition time = 500 Å / (evaporation rate before deposition). The sample #b1 is identical with #a3.

	(a) Evaporation rate dependence					(b) Substrate temperature dependence						
Sample Index	#a1	#a2	#a3	#a4	#a5	#b1	#b2	#b3	#b4	#b5	#b6	#b7
Evaporation rate† (Å/s)	**0.42**	**0.63**	**0.80**	**1.0**	**1.2**	0.80	0.83	0.82	0.84	0.83	0.83	0.83
Substrate temp. (°C)	45	45	45	45	45	**45**	**50**	**55**	**60**	**65**	**70**	**75**
Wall temp. (°C)	119	123	126	127	127	126	126	123	125	126	127	127
Source temp. (°C)	118	122	123	126	128	123	125	122	124	125	122	122
Vacuum ($\times 10^{-8}$ Torr)	3.1	4.9	2.1	4.7	3.0	2.1	3.1	4.6	2.6	3.5	3.2	2.6
Deposition time†† (s)	1240	826	624	475	426	624	626	614	626	609	616	618
Estimated thickness (Å)	520	520	500	490	500	500	520	500	520	510	510	510

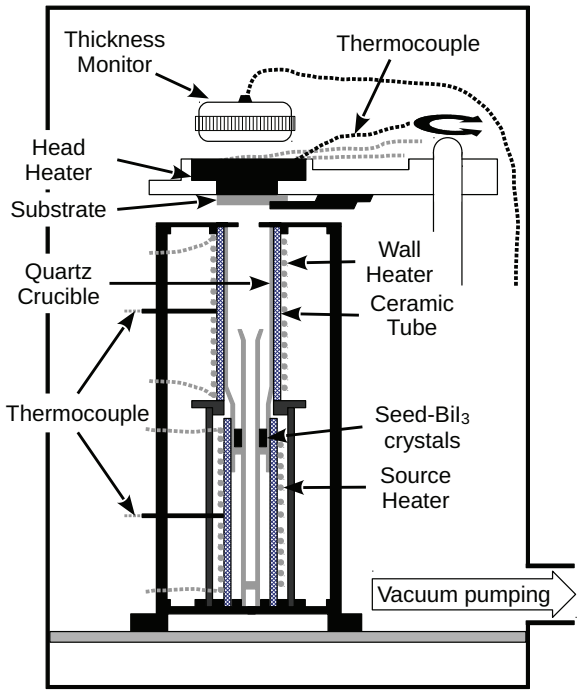

Figure 1 Schematic diagram of hot-wall furnace.

as shown in Fig. 1 and were evaporated by the source heater. The evaporation rate was stabilized by controlling the temperatures of the source and wall heaters, and it was monitored by a quartz crystal microbalance method with a thickness monitor and a crystal oscillation type deposition controller (CRTM-7000, ULVAC Inc.).

The conditions for the BiI_3 thin-film deposition are summarized in Table 1. The evaporation rate was determined by the averaged evaporation rate before and after sample deposition since the thickness monitor was screened by the substrate block during sample deposition as shown in Fig. 1. The ambient vacuum was kept at the order of 10^{-8} Torr. The deposition time was determined on the basis of the evaporation rate before deposition to be 500 Å/(evaporation rate before deposition) so that the deposited thickness being about 500 Å. For the samples #a1–#a5 in Table 1(a), the substrate temperatures were the same at $45°\mathrm{C}$, while the evaporation rates were varied from 0.42 Å/s to 1.2 Å/s. In the samples #b1–#b7 in Table 1(b), the evaporation rates were set to be about 0.8 Å/s and the substrate temperatures were varied from $45°\mathrm{C}$ to $75°\mathrm{C}$. The sample #b1 is identical to #a3.

Although the deposited thin films exhibit a dark brown color at room temperature, in the case of α-Al_2O_3 substrates, the thin films decolorize when stored at room temperature. This decolorization occurs peculiarly to α-Al_2O_3 substrates having a van der Waals surface, and it does not occur for other substrates of MgO-(111) surfaces and SiO_2. This decolorization is considered to be due to re-evaporation of deposited BiI_3 as a result of weak adsorptivity on the van der Waals surface of α-Al_2O_3. This shows that the van der Waals surface of α-Al_2O_3 is suitable for reducing the influence of the substrate during BiI_3 thin-film deposition. However, it was necessary to store the deposited samples in a freezer and all measurements had to be carried out promptly after thin-film deposition.

Out-of-plane XRD measurements were performed by θ-2θ scans at room temperature with an X-ray diffractometer (SmartLab, Rigaku Corp.) using a Cu-Kα line. The decolorization hardly occurred over the several hours of the XRD measurement. Absorption spectra were measured at 4 K using a cryostat (CF-1204, Oxford Corp.) and a spectrophotometer (V-650, JASCO Corp.).

3 Results

3.1 XRD Figures 2(a) and 2(b) show typical XRD data from out-of-plane measurements of the samples in Table 1(a) and 1(b), respectively. The ordinate for the diffraction intensity has a logarithmic scale and the abscissa is the diffraction angle 2θ. Figure 2(c) shows XRD data for the α-Al_2O_3 substrate for comparison and indicates that the diffraction peaks found at around 20° and 40° come from the α-Al_2O_3 substrate [30]. Diffraction peaks for the BiI_3 thin films are observed at the vertical dashed lines in Figs. 2(a) and 2(b), and correspond to diffraction from (0 0 $3m$) planes [31] ($m = 1 \sim 4$) in BiI_3. Tables 2(a) and 2(b) show the diffraction angles 2θ for the

Table 2 Diffraction angles 2θ in degrees for the (0 0 $3m$) planes ($m = 1 \sim 4$): (a) samples #a1–#a5, (b) sample #b1–#b7, (c) bulk crystal [29].

	(a) Evaporation rate dependence					(b) Substrate temperature dependence							(c) Bulk
Plane	#a1	#a2	#a3	#a4	#a5	#b1	#b2	#b3	#b4	#b5	#b6	#b7	
(003)	12.73	12.72	12.75	12.75	12.75	12.75	12.77	12.76	12.75	12.75	12.83	12.80	12.78
(006)	25.71	25.72	25.69	25.69	25.69	25.69	25.72	25.72	25.75	25.72	25.79	25.78	25.73
(009)	39.10		39.07	39.11	39.07	39.07	39.04	39.04	39.04	39.05	39.17	39.12	39.10
(0012)	52.87	52.84	52.84	52.89	52.89	52.84	52.90	52.92	52.96	52.92	53.02	53.05	52.95

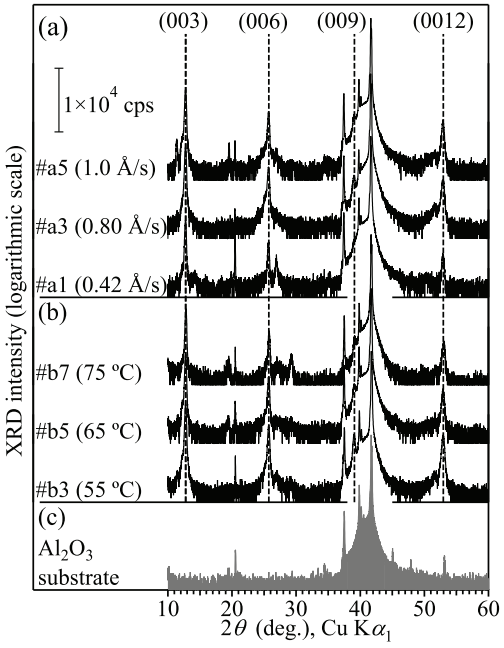

Figure 2 XRD data: (a) samples #a1, #a3 and #a5, (b) samples #b3, #b5 and #b7, (c) an α-Al_2O_3 substrate. The dashed lines in (a) and (b) show the diffraction angles of the (0 0 $3m$) planes ($m = 1$–4) in BiI_3.

(0 0 $3m$) planes in the respective samples #a1–#a5 and #b1–#b7, respectively. For comparison, the diffraction angles for the same planes in a BiI_3 single crystal are listed in Table 2(c) [29]. We can see that the diffraction angles for the same diffraction plane coincide within the accuracy range of the diffractometer. Focusing on the diffraction peak intensity, in the BiI_3 bulk crystal, the diffraction peak for the (003) plane is the strongest (0 0 $3m$) diffraction peak, and the intensity decreases with increasing m [29]. As can be seen in Fig. 2, a similar tendency can be confirmed in our samples. Since the (0 0 $3m$) planes are perpendicular to the stacking direction, the BiI_3 layers are stacked along the z-direction and it is confirmed that van der Waals epitaxy growth is realized by our hot-wall method.

3.2 Absorption spectra As described in the previous section, no noticeable changes were found in the regular XRD measurements depending on either evaporation rate or substrate temperature. To evaluate the homogeneity of the BiI_3 thin films, further advanced XRD and/or other atomic scale microscopic measurements are necessary. However, systematic changes were observed in the absorption spectra of the samples. Hence we evaluated the homogeneity of the BiI_3 thin films based on the changes in the absorption spectra. This is possible because the excitons providing the absorption peaks are strongly affected by the translational symmetry in the BiI_3 thin films [1,2,4, 27].

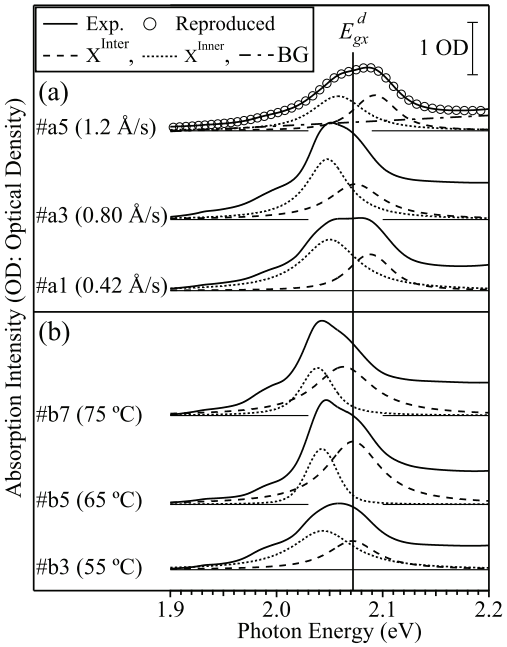

Figure 3 Absorption spectra: (a) samples #a1, #a3 and #a5, (b) samples #b3, #b5 and #b7. The spectral decomposition is described in Sec. 3.3.

Figure 3 shows typical absorption spectra at 4 K. The evaporation rates and substrate temperatures are denoted as indicated in the legend. The ordinate represents the absorption intensity in optical density (OD) and the abscissa is the photon energy in eV. Although it has been reported that the PV activity rises at $\sim$ 1.8 eV [20], no signifi-

cant spectral structure is found at $\sim$ 1.8 eV in the absorption spectrum of our thin films. As reviewed in [14], the absorption edge for high-quality BiI_3 single crystals is due to indirect exciton transitions at the transition energy $E_{gx}^{i} = 2.0081$ eV [32,33]. However, it is well known that various optical transitions appear at energies below E_{gx}^{i} due to stacking faults [14] and other causes. External strain is known to induce broad absorption bands around 1.9 eV [15], and they have been assigned to exciton transitions confined in mesoscopic domains produced by deformation faults with external strain [34]. It is believed that such strain does not occur in our thin films.

In high-quality BiI_3 single crystals, an intense absorption peak due to direct excitons appears at an energy slightly above E_{gx}^{i} [14]. In Fig. 3, the vertical solid line indicates the transition energy E_{gx}^{d} ($= 2.072$ eV [33,28]) for direct excitons at 4 K, and the dominant spectral peaks of the absorption spectra are considered to originate from the same direct excitons as in high-quality single crystals, although clear absorption bands due to indirect excitons cannot be detected around E_{gx}^{i} because of their weak absorption intensity. Instead of indirect absorption bands, a broad absorption band appears at about 1.99 eV below E_{gx}^{i} and this transition energy almost coincides with the transition energies for the SFE transitions R (1.9950 eV), S (1.9898 eV) and T (1.9856 eV), which are observed in bulk crystals [18] grown by a sublimation process. Although the R, S and T transitions have very narrow spectral widths of less than 1 meV [32] in high-quality bulk crystals, the absorption band due to SFEs becomes broad in our deposited samples, as seen in Fig. 3. Therefore, it is considered that the homogeneity is not high in the samples deposited by the hot-wall method.

As described in Sec. 2, although all the thin films were deposited assuming that the film thickness would be about 500 Å based on the product of the evaporation rate before deposition and the deposition time in Table 1, it is possible to discuss the actual thicknesses of the deposited BiI_3 thin films by examining the absorption intensity. It is found that the actual film thicknesses are approximately the same, because the spectral integrated absorption intensity has no significant dependence on the deposition conditions. This means that, within the current conditions in Table 1, evaporated BiI_3 molecules from the hot-wall furnace are stably supplied to the substrate, and re-evaporation from the substrate is not obvious. When the substrate temperature is too high, re-evaporation from the substrate would predominate and we are concerned that the deposited thin films would become thinner than 500 Å. However, even for sample #b7, deposited at the highest substrate temperature (75°C), the integrated absorption intensity does not decrease as seen in Fig. 3(b). This means that the deposited BiI_3 molecules are stably adsorbed on the substrate, within the temperature range from 45°C to 75°C.

3.3 Spectral decomposition In BiI_3/CdI_2 multilayer samples deposited by a hot-wall method, Watanabe *et al.* have studied splitting of direct excitons E_{gx}^{d} in BiI_3 [27]. They have argued that in such multilayer thin films, direct excitons split into inner $\mathrm{X}^{\mathrm{Inner}}$ and interface $\mathrm{X}^{\mathrm{Inter}}$ excitons because of the collapse of the translational symmetry in the stacking direction. The $\mathrm{X}^{\mathrm{Inner}}$ and $\mathrm{X}^{\mathrm{Inter}}$ exciton states have dominant envelop wavefunction amplitudes at the inside and the interfaced layers of the BiI_3 layers, respectively. A surface exciton [35,36] in the bulk BiI_3 crystal corresponds to the interface exciton in such multilayer samples. On the other hand, the inner exciton is a quantum confined state of the direct excitons and appears at a lower energy than E_{gx}^{d} because BiI_3 is an indirect-gap semiconductor.

Although similar splitting of direct exciton transitions are clearly observed in the respective absorption spectra in Fig. 3, their appearance changes noticeably depending on the sample. This change is considered to arise from differences in thin film morphology and quality. We have decomposed the main peak structure into two spectral components for the $\mathrm{X}^{\mathrm{Inner}}$ and $\mathrm{X}^{\mathrm{Inter}}$ excitons to examine the morphological changes. The spectral decompositions were performed by the least squares method. For the $\mathrm{X}^{\mathrm{Inner}}$ and $\mathrm{X}^{\mathrm{Inter}}$ exciton transitions, we employed Voigt line-shapes, which are convoluted Lorentzian line-shapes by Gaussian inhomogeneous broadening. In addition to these exciton transitions, a background (BG) component was taken into account. At energies higher than E_{gx}^{d}, absorption bands due to interband optical transitions and excited states of direct excitons appear and are superimposed as a gradual slope around E_{gx}^{d}. The BG component was approximated to be a linear function, and its parameters were selected and fixed to appropriate values. The spectral parameters for the Voigt functions have been optimized satisfactorily through minimization of the error function by the least squares method. In Fig. 3, the dashed and dotted lines indicate the spectral components for the $\mathrm{X}^{\mathrm{Inner}}$ and $\mathrm{X}^{\mathrm{Inter}}$ excitons, respectively. The dotted-dashed line in the uppermost spectrum (#a5) in Fig. 3(a) is the BG component. An example of the spectral reproduction is shown by the open circles for sample #a5 in Fig. 3(a). The curve represented by the open circles closely matches the measured absorption spectrum.

3.4 Deposition condition dependence We decomposed the absorption spectra for all the samples and could thus examine the systematic variations of the transition energies for the $\mathrm{X}^{\mathrm{Inner}}$ and $\mathrm{X}^{\mathrm{Inter}}$ excitons, where the respective transition energies are represented by E^{Inner} and E^{Inter}. Figures 4(a) and 5(a) show the dependence on the evaporation rate and substrate temperature, respectively. In these figures, the closed and open circles represent E^{Inner} and E^{Inter}, respectively.

The first important point in Fig. 4(a) is that E^{Inner} and E^{Inter} change in parallel with each other. This means that the energy difference ΔE ($\equiv E^{\mathrm{Inter}} - E^{\mathrm{Inner}}$) remains nearly constant, as indicated by the double-headed vertical arrow in Fig. 4(a). The mean value of ΔE for the samples

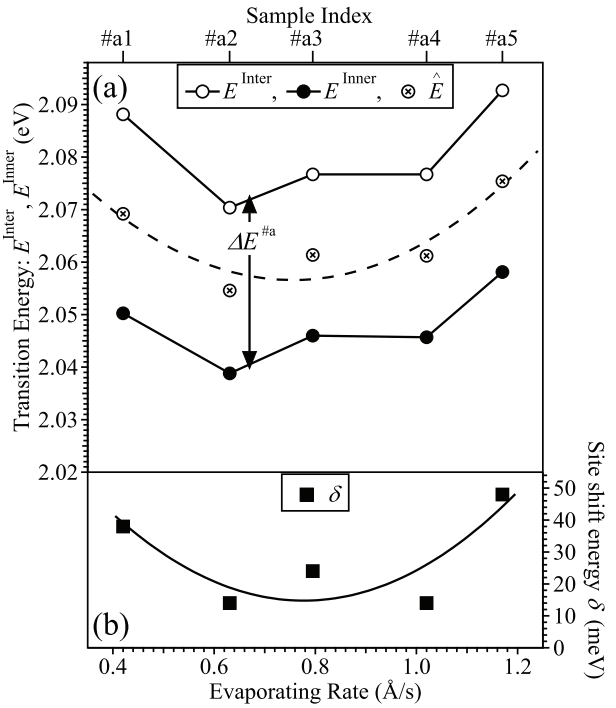

Figure 4 Evaporation rate dependence: (a) exciton transition energies $E^{\rm Inter}$ (○) and $E^{\rm Inner}$ (●), and $\hat{E}$ (⊗), (b) site shift energy δ.

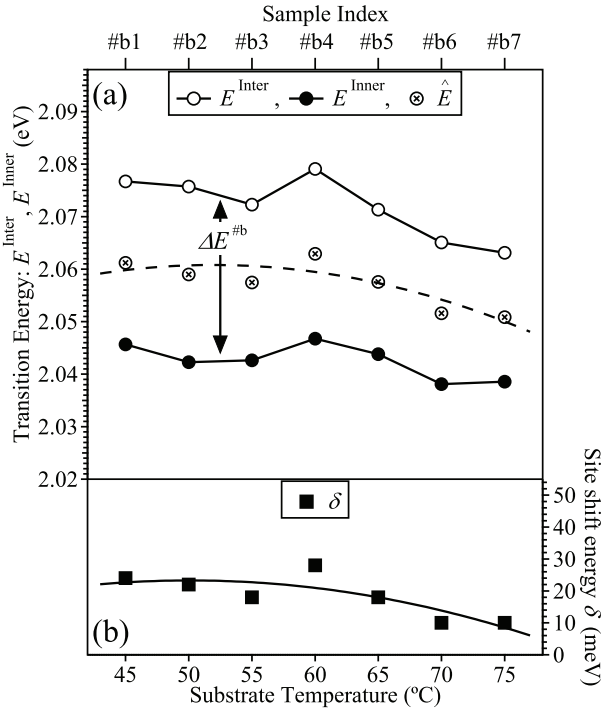

Figure 5 Substrate temperature dependence: (a) exciton transition energies $E^{\rm Inter}$ (○) and $E^{\rm Inner}$ (●), and $\hat{E}$ (⊗). (b) site shift energy δ.

#a1–#a5 is $\Delta E^{\#\rm a} = 33 \pm 1$ meV. The second important point is the variation of the mean value $\hat{E}$ ($\equiv (E^{\rm Inner} + E^{\rm Inter})/2$) of $E^{\rm Inner}$ and $E^{\rm Inter}$, plotted by the ⊗ symbols in Fig. 4(a). The dashed curve shows a fitting result for the $\hat{E}$ variation with a quadratic polynomial function of the evaporation rate, obtained by the least squares method. On the dashed curve in Fig. 4(a), $\hat{E}$ is minimized at an evaporation rate of about 0.8 Å/s.

In the substrate temperature dependence, a different trend is observed in the variation of the transition energies, as seen in Fig. 5(a). In the samples #b1–#b7, the mean value of ΔE is $\Delta E^{\#\rm b} = 29 \pm 1$ meV (the double-headed vertical arrow in Fig. 5(a)), and it is slightly smaller than $\Delta E^{\#\rm a}$. The transition energies $E^{\rm Inner}$ and $E^{\rm Inter}$ decrease monotonically with elevating substrate temperature, which is a significant different trend. In a similar way as for Fig. 4(a), the mean values $\hat{E}$ of the transition energies are plotted by the ⊗ symbols in Fig. 5(a) and the dashed curve shows the fitting of its variation as a function of substrate temperature.

By elevating the substrate temperature to approach the wall temperature, re-evaporation of bonded molecules at unstable sites predominates on the deposition surface of the BiI_3 thin film, while molecules bonded at more stable sites are considered to remain. Hence, it is expected that the homogeneity and crystallinity of the BiI_3 thin films will improve with elevating substrate temperature. It is therefore considered that the quality of the rightmost sample in Fig. 5(a), #b7, is higher than the other samples and that the low energy shift of $\hat{E}$ is an important signature of an improvement in sample quality. An evaporation rate of 0.8 Å/s is considered to be the best because, in Fig. 4(a), $\hat{E}$ is minimized for this evaporation rate at a substrate temperature of 45°C. Thus, for subsequent studies of the substrate temperature dependence, 0.8 Å/s was selected as the optimal evaporation rate.

4 Discussion In previous work [27] on BiI_3/CdI_2 multilayer structures, splitting of the direct exciton transition was analyzed by a tight-binding model. In this model, the differences in the transfer and on-site energies of direct excitons due to the collapse of the translational symmetry at the interface between BiI_3 and CdI_2 layers have been considered. In this section, we extend this tight-binding model for our samples and discuss variations of the sample morphology and quality.

4.1 Tight-binding model We assume that a BiI_3 thin film consists of flake-like crystals, and the flake-like crystal is formed by n fundamental BiI_3 layers, in which the translational symmetry for direct excitons is maintained in the regular stacking direction. Based on a previous study [27], an effective Hamiltonian $\mathcal{H}_n$ for direct excitons can be for-

mulated as Eq. (1).

$$\mathcal{H}_n = (\varepsilon+\delta)a_1^\dagger a_1 + T\,a_2^\dagger a_1 + \sum_{i=2}^{n-1}\left[\varepsilon a_i^\dagger a_i + T(a_{i-1}^\dagger a_i + a_{i+1}^\dagger a_i)\right] + T\,a_{n-1}^\dagger a_n + (\varepsilon+\delta)a_n^\dagger a_n, \quad (1)$$

where $a_i^\dagger$ and a_i ($i = 1 \sim n$) are creation and annihilation operators for direct excitons in the i-th BiI_3 layer, respectively. T is the transfer energy for direct excitons between neighboring BiI_3 layers. ε is the on-site energy for direct excitons in the respective BiI_3 layers. At the top and bottom BiI_3 layers ($i = 1$ or n) in the flake-like crystal, the on-site energy differs from that in the inside BiI_3 layers ($i = 2 \sim (n-1)$), where the difference is the site shift energy δ. ε and T can be determined based on the exciton band structure in BiI_3. In indirect gap semiconductors like BiI_3, the exciton band $\varepsilon(K)$ can be represented as $\varepsilon(K) = \varepsilon + 2T\cos(K\,a)$ [37] as a function of the excitonic wavenumber K by using T and ε, where a is the lattice constant. The exciton states at $K = 0$ and the band edge ($K = \pi/a$) correspond to the transition energies for direct excitons E_{gx}^d and indirect excitons E_{gx}^i, respectively. Thus, from the transition energies for both excitons at 4 K in BiI_3 crystals [28,33], T and ε can be determined as follows:

$$\varepsilon = \frac{1}{2}\left(E_{gx}^d + E_{gx}^i\right) = 2.040\ \mathrm{eV},$$
$$T = \frac{1}{4}\left(E_{gx}^d - E_{gx}^i\right) = 0.016\ \mathrm{eV}.$$

By diagonalizing $\mathcal{H}_n$, we can obtain the transition energies $\varepsilon^{\mathrm{Inner}}(n;\delta)$ and $\varepsilon^{\mathrm{Inter}}(n;\delta)$ for the inner $\mathrm{X}^{\mathrm{Inner}}$ and interface $\mathrm{X}^{\mathrm{Inter}}$ excitons, respectively, as functions of n and δ.

4.2 Number of fundamental layers n in the flake-like crystal can be estimated from the energy difference ΔE described in Sec. 3.4. Figure 6 shows an example of transition energies which vary depending on n. The open (△) and closed (▲) triangles show the $\varepsilon^{\mathrm{Inter}}$ and $\varepsilon^{\mathrm{Inner}}$, respectively, obtained from diagonalizations of $\mathcal{H}_n$ with $\delta = 20$ meV. The solid gray lozenges denote the energy difference $\Delta\varepsilon$ between $\varepsilon^{\mathrm{Inner}}$ and $\varepsilon^{\mathrm{Inter}}$. $\Delta\varepsilon$ clearly increases with decreasing n, where this trend in $\Delta\varepsilon$ is assured even if δ is changed.

In Sec. 3.4, we obtained $\Delta E^{\#\mathrm{a}}$ ($= 33 \pm 1$ meV) and $\Delta E^{\#\mathrm{b}}$ ($= 29 \pm 1$ meV), denoted by the double-headed vertical arrows in Fig. 4(a) and 5(a), respectively. $\Delta E^{\#\mathrm{a}}$ and $\Delta E^{\#\mathrm{b}}$ are indicated on the right ordinate for $\Delta\varepsilon$ in Fig. 6. From the agreement between $\Delta E^{\#\mathrm{a}}$ and $\Delta\varepsilon$, it is considered that the samples #a1–#a5 consist of flake-like crystals formed by four ($n = 4$) BiI_3 layers. The samples #b1–#b7 are expected to be flake-like crystals formed from more than four BiI_3 layers because $\Delta E^{\#\mathrm{b}}$ is slightly smaller than $\Delta E^{\#\mathrm{a}}$ and is between $\Delta\varepsilon(n = 4)$ and $\Delta\varepsilon(n = 5)$, as seen in Fig. 6. However, since the thickness of a BiI_3 layer is 6.89 Å [26], a BiI_3 thin film should consist of a total of about 70 (≈ 500 Å/6.89 Å) BiI_3 layers based on the estimated thicknesses of about 500 Å. This discrepancy between n and the total number of layers in the film indicates that the translational symmetry is not maintained over the whole thickness (about 500 Å) and it is considered that many flake-like crystals are packed in the BiI_3 thin film. In these flake-like crystals, the translational symmetry is maintained within four or five BiI_3 layers (about 27.6 Å or 34.5 Å) as analyzed in this section.

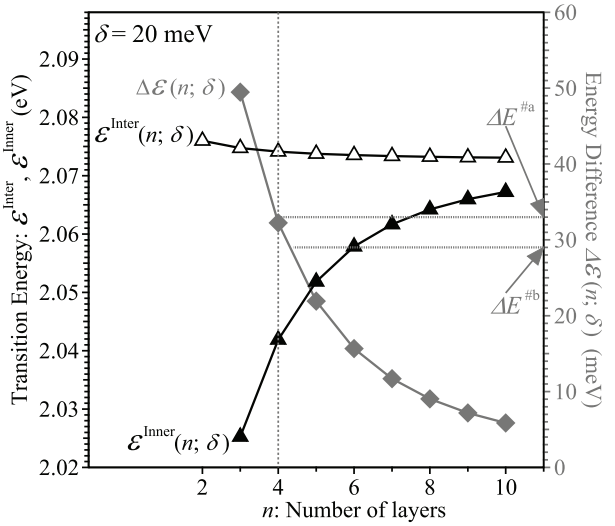

Figure 6 Transition energies $\varepsilon^{\mathrm{Inner}}$ (▲) and $\varepsilon^{\mathrm{Inter}}$ (△) as functions of the fundamental layer number n with $\delta = 20$ meV. The solid gray lozenges show the energy differences $\Delta\varepsilon$ between $\varepsilon^{\mathrm{Inner}}$ and $\varepsilon^{\mathrm{Inter}}$.

To realize SFE states with high homogeneity, it is essential that a homogeneous 2D-space consists of three fundamental layers sandwiching the stacking fault interface [16]. Hence, we should improve the translational symmetry continuity in the stacking direction in order to control the stacking fault formations by the hot-wall method.

4.3 Site shift energy In Sec. 4.2, we considered that the translational symmetry is maintained within four or five BiI_3 layers in the flake-like crystals. On the other hand, the packing density among the flake-like crystals can be evaluated from δ. In Figs. 4(a) and 5(a), the mean value $\hat{E}$ (⊗) for the transition energies varies systematically and this variation arises from the change of δ as described below.

In Fig. 7(a), $\varepsilon^{\mathrm{Inner}}$ and $\varepsilon^{\mathrm{Inter}}$ are plotted as functions of δ by closed and open triangles, respectively. The black and gray colors denote $n = 4$ and 5, respectively. The ⊗ and ⊕ symbols display the mean value $\hat{\varepsilon}$ ($\equiv [\varepsilon^{\mathrm{Inter}} + \varepsilon^{\mathrm{Inner}}]/2$) for $n = 4$ and 5, respectively. As seen in Fig. 7(a), $\hat{\varepsilon}$ increases monotonically with increasing δ for both values of n. In Fig. 7(a), the arrows pointing to the left ordinate, labeled $\hat{E}_{\mathrm{min.}}^{\#\mathrm{a}}$ and $\hat{E}_{\mathrm{min.}}^{\#\mathrm{b}}$, indicate the minimum values of

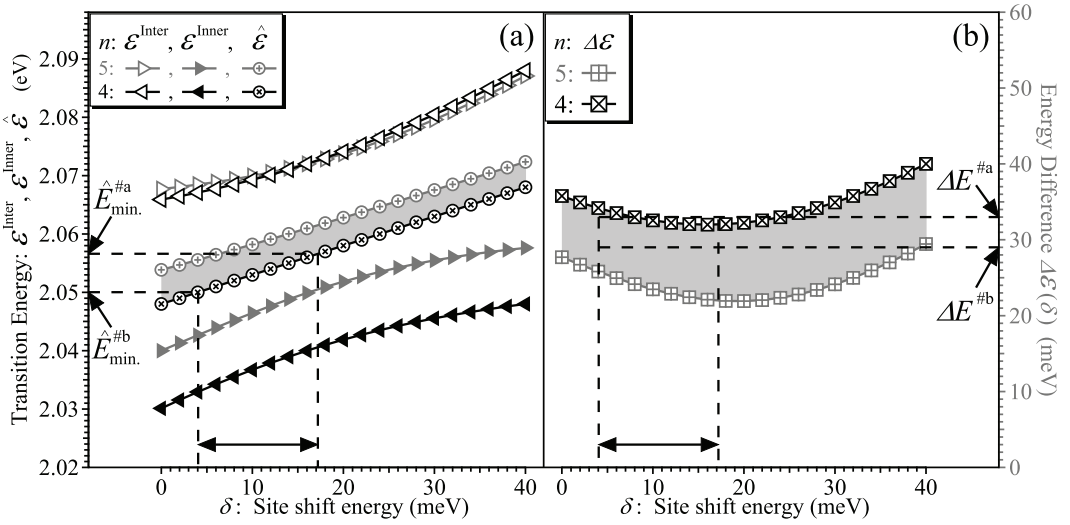

Figure 7 (a) Transition energies $\varepsilon^{\mathrm{Inner}}$, $\varepsilon^{\mathrm{Inter}}$ and their mean value $\hat{\varepsilon}$ as functions of the site shift energy δ. (b) Energy differences $\Delta\varepsilon$ as functions of δ. The black and gray points represent BiI_3 layer numbers of $n = 5$ and 4, respectively.

the dashed curves in Figs. 4(a) and 5(a), respectively. As described in the last paragraph of Sec. 3.4, $\hat{E}$ shifts to lower energy as the sample quality improves. Therefore, from the agreement between $\hat{\varepsilon}$ and these minimum values ($\hat{E}^{\#\mathrm{a}}_{\mathrm{min.}}$ and $\hat{E}^{\#\mathrm{b}}_{\mathrm{min.}}$), we can determine δ values under the best conditions for the respective sample groups #a1–#a5 and #b1–#b7 and the difference between $\hat{E}^{\#\mathrm{a}}_{\mathrm{min.}}$ and $\hat{E}^{\#\mathrm{b}}_{\mathrm{min.}}$ corresponds to a change of δ from 4.1 meV to 17 meV in the case of $n = 4$, as shown by the double-headed horizontal arrow in Fig. 7(a).

This change in δ can be understood from the viewpoint of the δ-dependence of $\Delta\varepsilon$. The black (⊠) and gray (⊞) points in Fig. 7(b) show $\Delta\varepsilon$ as a function of δ for $n = 4$ and 5, respectively. In Sec. 3.4, ΔE was obtained from spectral decomposition, and the values of $\Delta E^{\#\mathrm{a}}$ and $\Delta E^{\#\mathrm{b}}$ are indicated by the arrows on the right ordinate in Fig. 7(b). $\Delta E^{\#\mathrm{a}}$ matches $\Delta\varepsilon(n = 4)$ in the same δ range (4.1–17 meV). Although $\Delta E^{\#\mathrm{b}}$ is less than $\Delta\varepsilon(n = 4)$ in the same δ range, the gray area contains this value as seen in Fig. 7(b), where the gray area indicates the range of $\Delta\varepsilon$ between $n = 4$ and $n = 5$. This result is reasonable because the samples #b1–#b7 consist of flake-like crystals of more than four ($n = 4$) BiI_3 layers, as discussed in Sec. 4.2.

We now discuss the magnitude of δ. When the translational symmetry is completely maintained, $\delta = 0$ is strikingly apparent since they are not interface layers. In contrast, a large site shift energy of about 80 meV [27] has been reported for surface excitons [36] of BiI_3 bulk crystals. In BiI_3/CdI_2 multilayer samples, it has been reported that the site shift energy for interfaced layers with CdI_2 decreases to about 47 meV [27]. In our BiI_3 thin films, δ further decreases and asymptotically approaches zero. This result suggests that very similar substances adjoin just outside the flake-like crystals. Therefore, it is considered that, in our BiI_3 thin films, the flake-like crystals are surrounded by other flake-like crystals and some derivatives of BiI_3. However, because of the finite value of δ, it is evident that the translational symmetry collapses at the adjoining boundary.

4.4 Improvement of deposition conditions As discussed in Sec. 4.3, δ varies in accordance with the packing density and/or uniformity of other BiI_3 substances surrounding the flake-like crystals, and will approach zero through improvements in sample quality. The black square symbols in Figs. 4(b) and 5(b) show the variation of δ with the deposition conditions. The solid lines are fitting results of δ variations with quadratic polynomial functions by the least squares method. As seen in Fig. 4(b), δ has a minimum value at an evaporation rate of about 0.8 Å/s, similar to $\hat{E}$ (⊗) in Fig. 4(a). In Fig. 5(b), δ also decreases monotonically with increasing substance temperature. Thus, a further asymptotic approach to zero is expected as the substrate temperature approaches the wall temperature (119°C–127°C).

In conclusion, it is found that an evaporation rate of 0.8 Å/s and substrate temperature of 75°C are the best conditions for BiI_3 thin film deposition on α-Al_2O_3 substrates. However, as discussed in Secs. 4.2 and 4.3, translational symmetry of the regular stacking is assured only within four or five BiI_3 layers, and the thin films are formed by packing of such flake-like crystals. It is hence important to improve the thin film quality to control stacking fault formation in BiI_3 by the hot-wall method.

5 Summary By using a hot-wall method, BiI_3 thin films were deposited on α-Al_2O_3 substrates. To optimize the deposition conditions, the evaporation rate (#a1–#a5) and substrate temperature (#b1–#b7) were varied in the

ranges of 0.42–1.2 Å/s and 45–75°C, respectively. The sample quality was studied based on XRD data and excitonic absorption spectra.

The XRD data showed that thin-film growth by van der Waals epitaxy is realized in the BiI_3 thin films. An absorption peak due to direct excitons in BiI_3 can be decomposed into inner X^{Inner} and interface X^{Inter} excitons, and the mean values $\hat{E}$ and the differences ΔE of their transition energies E^{Inner} and E^{Inter} were analyzed. We discussed the deposition condition dependence on $\hat{E}$ and ΔE based on the tight-binding model, which explains the inner and interface excitons in flake-like crystals. In the flake-like crystals, it was considered that the translational symmetry along the stacking direction is maintained within a finite number of BiI_3 layers (the layer number being denoted by n) and we introduced the site shift energy δ at the interfaces between the flake-like crystals. The energy difference $\Delta E^{\#a}$ for the samples #a1–#a5 deposited at a substrate temperature of $45°C$ matched the calculated result $\Delta\varepsilon(n = 4)$. In the samples #b1–#b7 deposited at higher substrate temperatures, the energy difference $\Delta E^{\#b}$ was smaller than $\Delta E^{\#a}$ and was located between $\Delta\varepsilon(n = 4)$ and $\Delta\varepsilon(n = 5)$. These results suggest that the flake-like crystals consist of four and five BiI_3 layers and that the thin films are formed by the packing of such flake-like crystals. On the other hand, the mean value $\hat{E}$ varies systematically depending on the evaporation rate in the samples #a1–#a5 and on the substrate temperature in the samples #b1–#b7. According to the tight-binding model, the variation of δ can explain the variations in $\hat{E}$. For the samples #a1–#a5, the value of δ obtained from $\hat{E}^{\#a}$ has a minimum value at an evaporation rate of about 0.8 Å/s. In the samples #b1–#b7, δ decreases monotonically with increasing substrate temperature. Since the decrease toward zero of δ is thought to represent an improvement in the sample quality, it can be considered that in our hot-wall method, an evaporation rate of 0.8 Å/s and substrate temperature of $75°C$ are the best conditions for BiI_3 thin film deposition on α-Al_2O_3 substrates.

Acknowledgements This work was supported by Kakenhi Grants-in-Aid (Nos. 16H01552, 16H04002, and 16K13824) from the Japan Society for the Promotion of Science (JSPS).

References

[1] R. S. Knox, *'Theory of Excitons'*, *Academic Press Inc.*, (1963).
[2] E. I. Rashba, M. D. Sturge (Eds.), *'Excitons: Selected Chapters (Modern Problems in Condensed Matter Sciences)'*, *Elsevier Science Ltd.*, (1987).
[3] H. Haug, S. W. Koch, *'Quantum Theory of the Optical and Electronic Properties of Semiconductors, 2nd ed.'*, *World Scientific Pub. Co. Inc.*, (1993).
[4] T. Ogawa, Y. Kanemitsu (Eds.), *'Optical Properties of Low-Dimensional Materials'*, *World Scientific Pub. Co. Inc.*, (1995).
[5] L. L. Chang, L. Esaki, *Phys. Rev. Lett.* **33**, 495 (1974).
[6] A. Y. Cho, *Phys. Rev. Lett.* **19**, 467 (1971).
[7] D. P. Daniel, *Annu. Rev. Mat. Sci.* **19**, 467 (1971).
[8] A. Mysyrowicz, D. Hulin, A. Antonetti, A. Migus, W. T.Masselink, H. Morkoç, *Phys. Rev. Lett.* **56**, 2748 (1986).
[9] A. K. Geim, K. S. Novoselov, *Nat. Mat.* **6**, 183 (2007).
[10] A. H. Castro Neto, F. Guinea, N. M. R. Peres, K. S. Novoselov, A. K. Geim, *Rev. Mod. Phys.* **81**, 109 (2009).
[11] J. S. Ross, S. Wu, H. Yu, N. J. Ghimire, A. M. Jones, G. Aivazian, J. Yan, D. G. Mandrus, D. Xiao, W. Yao, X. Xu, *Nat. Commun.* **4**, 1474 (2013).
[12] M. M. Ugeda, A. J. Bradley, S.-F. Shi, F. H. da Jornada, Y. Zhang, D. Y. Qiu, W. Ruan, S.-K. Mo, Z. Hussain, Z.-X. Shen, F. Wang, S. G. Louie, M. F. Crommie, *Nat. Mater.* **13**, 1091 (2014).
[13] K. He, N. Kumar, L. Zhao, Z. Wang, K. F. Mak, H. Zhao, J. Shan, *Phys. Rev. Lett.* **113**, 026803 (2014).
[14] Y. Kaifu, *J. Lumin.* **42**, 61 (1988).
[15] Y. Kaifu, T. Komatsu, T. Aikami, *Nuovo Cimento* **38 B**, 449 (1977).
[16] T. Komatsu, Y. Kaifu, S. Takeyama, N. Miura, *Phys. Rev. Lett.* **58**, 2259 (1987).
[17] I. Akai, T. Karasawa, Y. Kaifu, *J. Phys. Soc. Jpn.* **58**, 718 (1989).
[18] I. Akai, T. Karasawa, T. Komatsu, Y. Kaifu, *Phys. Rev. B* **43**, 4484 (1991).
[19] T. Karasawa, T. Kawai, H. Mino, I. Akai, T. Komatsu, *J. Lumin.* **72-74**, 876 (1997).
[20] R. E. Brandt, R. C. Kurchin, R. L. Z. Hoye, J. R. Poindexter, M. W. B. Wilson, S. Sulekar, F. Lenahan, P. X. T. Yen, V. Stevanović, J. C. Nino, M. G. Bawendi, T. Buonassisi, *J. Phys. Chem. Lett.* **6**, 4297 (2015).
[21] P. M. Johns, S. Sulekar, S. Yeo, J. E. Baciak, M. Bliss, J. C. Nino, *J. Cryst. Growth* **433**, 153 (2016).
[22] W. Qiu, G. J. Dudder, X. Zhao, S. S. Perry, J. C. Nino, *ACS Appl. Mater. Interfaces* **3**, 1910 (2011).
[23] A. Koma, K. Sunouchi, T. Miyajima, *Microelectronic Eng.*, **2**, 129 (1984).
[24] S. Takeyama, K. Watanabe, T. Komatsu, *Jap. J. Appl. Phys.*, **29**, 710 (1990).
[25] S. Takeyama, K. Watanabe, M. Ichihara, K. Suzuki, N. Miura, *J. Apple. Phys.* **68**, 2735 (1990).
[26] R. W. G. Wyckoff : *Crystal Structure* (Interscience, New York, 1963) 2nd ed. **1**, 266; *ibid.* (1964) **2**, 45.
[27] K. Watanabe, N. Miura, T. Komatsu, *J. Phys. Soc. Jpn.* **63**, 4213 (1994).
[28] T. Komatsu, Y. Kaifu, *J. Phys. Soc. Jpn.*, **40**, 1062 (1976).
[29] H. E. Swanson, N. T. Gilfrich, M. I. Cook, *NBS Circular 539,* **6**, 20 (1956).
[30] T. C. Huang, W. Parrish, N. Masciocchi, P. Wang, *Adv. X-Ray Anal.* **33**, 295 (1990).
[31] M. Ruck, *Z. Kristallogr.* **210**, 650 (1995).
[32] Y. Kaifu, T. Komatsu, *J. Phys. Soc. Jpn.* **40**, 1377 (1976).
[33] T. Karasawa, T. Komatsu, Y. Kaifu, *Solid State Commun.* **44**, 323 (1982).
[34] T. Komatsu, T. Iida, K. Murayama, M. Ichida, H. Kurisu, H. Kondo, I. Akai, T. Karasawa, *Mol. Cryst. Liq. Cryst.* **218**, 37 (1992).

[35] T. Komatsu, T. Karasawa, Y. Kaifu, T. Iida, *Physica* **99B**, 318 (1982).
[36] K. Watanabe, S. Takeyama, N. Miura, T. Komatu, *Solid State Commun.* **74**, 37 (1994).
[37] C. Kittel, *Introduction to Solid State Physics, 7th ed.*, John Wiley & Sons, Inc. (1996).